Lowland Technology International 2017; 19 (1): 1-12
International Association of Lowland Technology (IALT): ISSN 1344-9656

Research Paper

Three dimensional (3D) failure pattern of flexible pile due to lateral cyclic loading in sand

M. F. Awad-Allah [1], N. Yasufuku [2] and S. Manandhar [3]

ARTICLE INFORMATION

Article history:

Received: 22 February, 2017
Received in revised form: 16 March, 2017
Accepted: 21 March, 2017
Publish on: 07 June, 2017

Keywords:

Photo image analysis
Flexible piles
Plastic deformation
Lateral cyclic loading
Sand

ABSTRACT

In this paper, a set of small-scale laboratory single flexible pile model was conducted in a medium dense Toyoura sand environment under the effect of cyclic lateral loads. Digital images were captured for the plastic deformations of the soil during the lateral loading from the top of the testing chamber. Combination of photo image analysis and analytical cyclic p-y curve methods was implemented for estimating the three dimensional (3D) failure zone adjacent to pile shaft. The 3D failure pattern of the soil around single pile shaft was investigated through two steps, including: (1) determination of the range of lateral plastic deformations at the top of ground surface in perpendicular and parallel directions of cyclic loads; and (2) determination of the point of rotation (zero displacement) along the pile shaft. Experimental results showed that a conical passive zone of plastic deformations is established around pile shaft due to applying two-way lateral cyclic loading at pile head. Based on the findings, design considerations for piles subjected to lateral cyclic loading have been introduced.

1. Introduction

Pile foundations are commonly subjected to cyclic lateral loading which often arise from earthquake, wind, waves, etc. Some examples of structures that are mainly subjected to lateral cyclic loading including: jetties, wind turbine, and harbor structures, and pile foundations located in seismic zones and piers supported by piles.

Significant amount of research has been conducted for many years to formulate the design of pile foundations supporting lateral cyclic loads, owing to its critical relevance to foundation engineering under demanding structural, soil, and loading conditions (Abedzadeh and Pak, 2004). Most of the theoretical solutions for laterally loaded piles involve the concept of modulus of subgrade reaction which is based principally on Winkler's assumption. Within this framework, Reese (1977) proposed the well-known p-y curve method. This approach is based on the differential equation for solving the problem of the laterally loaded pile (Eq. 1), and it can be used for both free- and fixed-head single piles. By means of finite-element, boundary-element, or finite-difference methods, numerical solutions can also be obtained for this class of problems.

$$p = EI\frac{d^4y}{dz^4} \quad [1]$$

where: EI = bending (flexural) stiffness of pile, y = lateral displacement, z = depth below the ground surface,

[1] Researcher, Ph.D., Department of Civil Engineering, National Research Center, EGYPT, ORCID ID 0000-0002-0370-6282, mahmoud_fawzi@hotmail.com
[2] Professor, Geotechnical Laboratory, Department of Civil Engineering, Faculty of Engineering, Kyushu University, 744 Motooka, Nishi-ku, Fukuoka, 819-0395, JAPAN, yasufuku@kyushu-u.ac.jp
[3] Head of Department, Associate Professor & IALT member, Department of Disaster Risk Engineering and Management, Lumbini International Academy of Science and Technology, Lumbini Buddhist University, NEPAL, geosuman27@gmail.com
Note: Discussion on this paper is open until December 2017

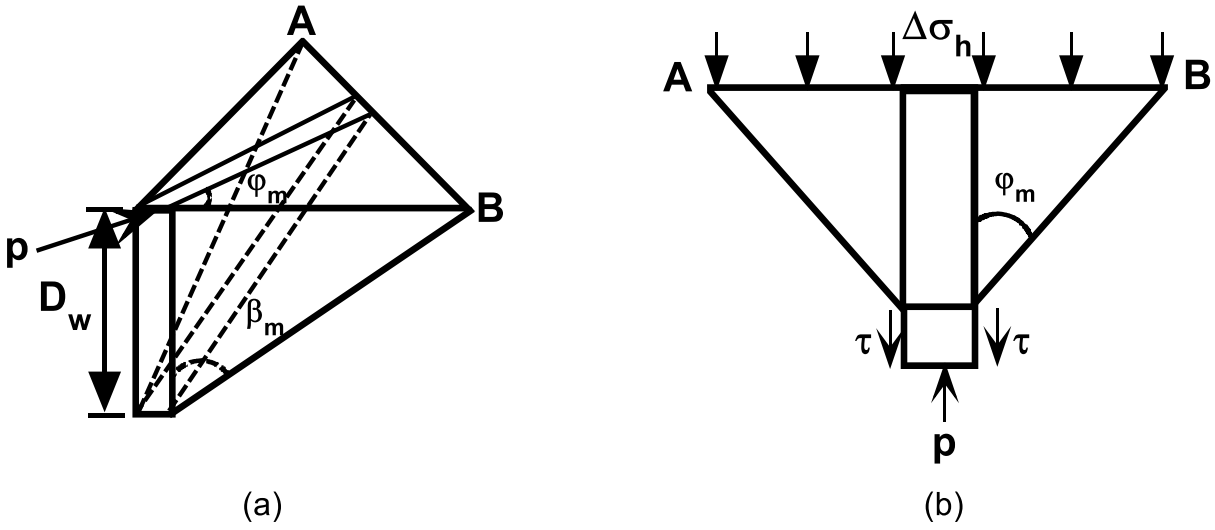

Fig. 1. Failure pattern around laterally loaded pile (after Reese et al, 1974): (a) cross-section, and (b) plan.

and p = soil reaction per unit length of pile.

According to the earth pressure theory, the lateral stress at fully mobilized passive state is equal to Kp times vertical effective stress. For laterally loaded piles, however, the magnitude of the ultimate lateral soil resistance (p_u) is much greater than Rankine's passive stress due to the three dimensional characteristics of the lateral soil resistance (Fleming et al., 2009). Owning to pile under lateral load is a typical three dimensional problem, some researchers investigated the 3D failure patterns in sand due to static laterally loaded pile (e.g. Otani et al., 2006; Ashour and Norris, 1998; Kishida and Nakai, 1979; and Reese et al., 1974).

Ashour and Norris (1998) employed the visualized 3-D strain wedge (SW) model, which was developed by Reese et al. (1974), and Kishida and Nakai (1979) to determine pile response to static lateral loads, as shown in **Fig. 1a**. The SW model was capable of linking between the more complex 3D soil-pile interaction and a simpler one-dimensional characterization. In this method, the SW properties are characterized by base angles (β_m), passive wedge depth (DW), and spread of wedge angle (φ_m, the mobilized friction angle). The horizontal stress change at the passive wedge face ($\Delta\sigma_h$) and the side shear (τ) act on the strain wedge are presented in **Fig. 1b**.

Based on image analysis by particle image velocimetry (PIV) method, Masoud et al. (2011) investigated the maximum shear strain created in soil around a single pile subjected to lateral loads. It was observed that the maximum shear strain occurred in pile adjacent to soils near the surface as shown in **Fig. 2a** that a triangular strain wedge to the side of the displaced pile is created, and **Fig. 2b** shows that in front of a laterally loaded pile a passive zone is established which it is similar to circle. By composing **Figs. 2a** and **2b** it is concluded that front of a laterally loaded pile, the passive zone that is established is almost conical in shape in three dimensions. Moreover, Otani et al. (2006) used X-ray computed tomography (CT) scanner for visualizing failure pattern of the ground (sand) around a pile owing to a lateral load. In this research, they showed that the size of failure zone decreases with the increase in the ground depth along the pile shaft and the shape of this failure zone is almost conical in three dimensions. An image processing analysis was conducted to obtain effective CT images. Based on the images, 3D failure patterns of the ground under laterally loaded piles were visualized (**Fig. 3**).

2. Experimental setup

2.1 Testing apparatus and pile model

Figure 4 shows the test set-up along with the assembly of the lateral loading device and measurement equipment for single pile test. The soil testing chamber is made of rigid fiberglass plates of wall thickness equal to 5 cm. In order to prevent the artificial boundary effect (i.e. side and end walls) during testing, the length to height ratio (l/h) of the container was designed to be in the range of 1.5-2.0; therefore, the testing box has a length to height (l/h) ratio of 1.58 (Lombardi et al., 2015). Moreover, the measuring apparatus include strain gauges, linear variable displacement transducers (LVDTs) and load cell. Lateral cyclic load was applied on

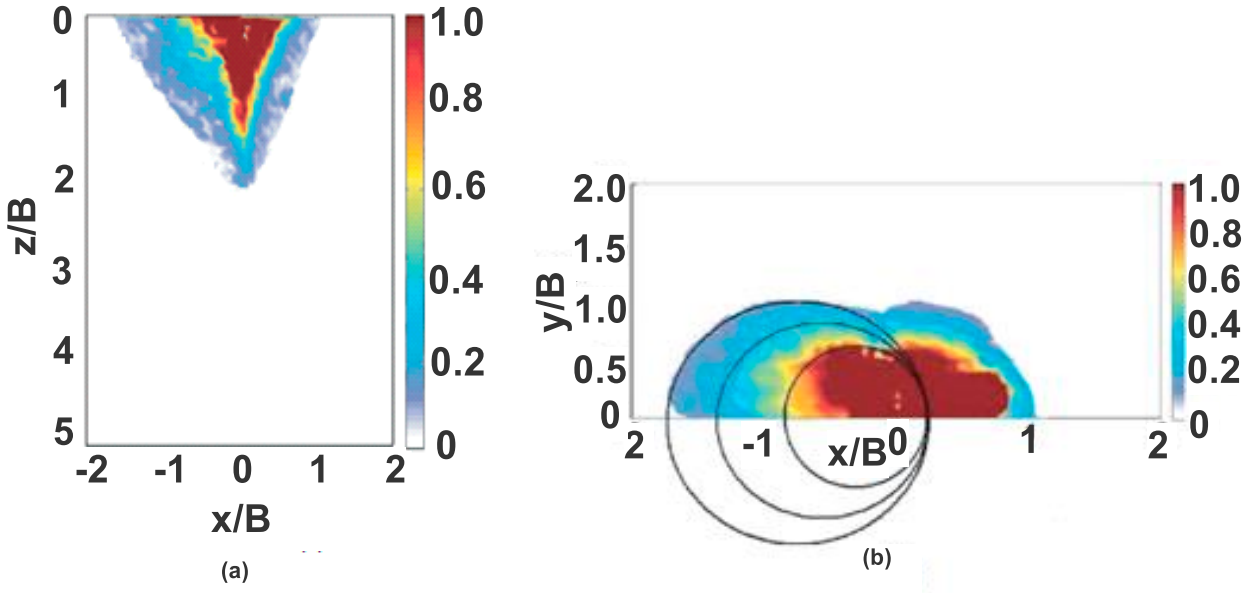

Fig. 2. Soil shear strain around pile: (a) side view and (b) plan.

the pile head by means of a servo cylinder which was totally fixed in pile cap by way of steel screw bolts. An external control unit was used to control the number of applied cycles (N) and loading frequencies (f). The pile model was manufactured from a closed-end aluminum alloy 6061 tube of outer diameter 15 mm and wall thickness 1.5 mm. The Young's modulus and yield stress of the used aluminum alloy are 70 GPa and 48.3 MPa, respectively. Furthermore, two different slenderness ratios (L/B = 20 and 30) for pile model were selected for testing.

2.2 Testing ground (soil)

Testing soil used in this laboratory work, is sub-angular, fine Toyoura sand, which is commonly used as testing soil in Japan, and its index properties are given in **Table 1**. Since the ratio of pile diameter to effective diameter of soil (B/D50) is about 83.33, which is comfortably greater than the minimum value of 40 usually recommended by Ovesen (1975), the sand would behave like a continuum as would be the case in the prototype.

Furthermore, mini-cone penetration tests were carried out according to JGS 1431 (2003) after soil placement over the whole depth of the testing box (60cm) at three different locations inside the testing tank, as depicted in **Fig. 5**. Based on the obtained results of cone penetration resistances (q_c), the strength and deformation properties of the ground soil can be estimated using the empirical correlations introduced by Nikudel et al. (2012). **Figure 5** shows the results of Mini-cone penetration resistance test (q_c) with depth (z) for the three conducted tests, which gives the following average physical soil properties of sand: Young's modulus (Es), and internal friction angle (φ) of 6.48 MPa, and 36.5°, respectively.

Multiple sieving pluviation (MSP) method, which was developed by Miura and Toki (1982), was used for preparation of sand samples. This method has some advantages over standard compaction method, including: (1) protecting strain gauges attached to piles from damage, and (2) producing homogenous testing ground around pile.

2.3 Physical modeling and scaling laws

Physical modeling plays a fundamental role in the development of geotechnical understanding. If the physical modeling is to be performed at any scale other than full scale, then the key question is concerned with establishing the validity of the models and ensuring that the extrapolation principle can be extended from the behavior studied at model scale to the behavior expected at prototype scale. The understanding of relevant scaling laws and the dimensional analysis, which controls them, is essential. Examples of derivation of scaling laws for general dynamic problems are proposed by Wood et al. (2004).

The equation governing the lateral deformation of the pile under lateral load, given previously in Eq. 1, can be written in the following form:

$$EI\frac{d^4y}{dz^4} = -K_h * y \qquad [2]$$

where: K_h = subgrade reaction modulus.

A natural dimensionless ratio $\phi_1=K_hL^4/EI$ to characterize the problem is employed, which describes the relative pile-soil stiffness parameter. Then it might be supposed that correct physical modeling will be obtained if the dimensionless ratio ϕ_1 is maintained as identical in the model and the prototype (Bhattacharya et al., 2011). For granular soils, the stiffness property of the soil is roughly proportional to the square root of the vertical effective stress of soil, $\sigma_v=(\gamma z)^{0.5}$, and then $K_h= n_h (z)^{0.5}$ in which n_h is the constant of the modulus horizontal subgrade reaction. In this case, the dimensionless ratio for 1g test in granular soil can be considered as $\phi_1= K_hL^{4.5}/EI$ (i.e., 4 for pile flexural stiffness plus 0.5 to account for change in soil stiffness). This leads to general scaling law, as given in (Eq. 8).

$$\left(\Phi_1\right)_m = \frac{n_h L_m^{4.5}}{E_m I_m} \quad [3]$$

$$\left(\Phi_1\right)_p = \frac{n_h L_p^{4.5}}{E_p I_p} \quad [4]$$

$$\frac{\left(\Phi_1\right)_p}{\left(\Phi_1\right)_m} = \frac{L_p^{4.5}.I_m E_m}{L_m^{4.5}.I_p E_p} \quad [5]$$

$$\frac{E_m I_m}{E_p I_p} = \frac{L_m^{4.5}.}{L_p^{4.5}.} \quad [6]$$

$$\frac{L_m}{L_p} = \frac{1}{F.} \quad [7]$$

$$\frac{E_m I_m}{E_p I_p} = \frac{1}{F^{4.5}} \quad [8]$$

where: E_mI_m = Flexure rigidity of model pile material; E_pI_p = Flexure rigidity of prototype pile; L_m = embedded length of model pile; L_p = embedded length of prototype pile; and F = L_p/L_m = scale factor for length.

In this experimental work, scaling factor for length is adopted as (L_p/L_m = F = 20) based on previous work of Chandrasekaran et al. (2010). Therefore, the value of scaling factor for pile length will be equal to ($1/F = 1/20^{4.5}$). Hence, if an aluminum tube pile model of outer diameter 15mm and wall thickness 1.5mm is used, it will be equivalent to a prototype of circular steel pipe pile of outer diameter 600 mm and wall thickness of 6 mm.

Table 2 shows the relevant parameters for the prototype and the laboratory model. It is obvious that the prototype has been scaled down in terms of stress and length by values of 3 and 40, respectively. Although the geostatic stress does not match the prototype scale, the stiffness of the pile is reduced too. Therefore, the modeling is valid for the interaction of soil and pile.

2.4 Relative system of pile-soil system

The relative stiffness factor K_{rs} is calculated for the pile models using the equation proposed by Poulos and Davis (1980). For flexible piles, the value of K_{rs} is smaller than 10^{-2}.

$$K_{rs} = \frac{E_m I_m}{E_s L^4} \quad [9]$$

The calculated values of (K_{rs}) for those piles used in this experimental scheme were 0.0019 and 0.0004 for slenderness ratios (L/B) of 20, and 30, respectively. Hence, the piles used in this study were considered as flexible piles.

3. Visualization of lateral deformation at top soil surface

3.1 Test procedures and protocol

The procedures given below were conducted for preparing the laboratory model test. Pile model was placed at the center of the cleaned testing chamber by clamping it against the guide bar to avoid boundary effect. Meanwhile examination of its vertical alignment is performed. Then, sand was poured in carefully, slowly, and evenly on layers of 10 cm in thickness. After reaching to the uppermost layer of sand, the guide beam was removed and the top surface was flattened.

In this testing program, two-way cyclic lateral displacement was imposed on the pile head based on the cyclic loading pattern recommended by Basack and Purkayasthab (2007); and LeBlanc et al. (2010). The head of the tested pile was pushed forward *laterally* by 3 mm (i.e., 10% of pile outer diameter), then it is pulled back in the opposite direction by 6 mm, and then it is pushed back by 3mm (i.e., set back to initial position), as shown in **Fig. 6**. The cyclic loading direction was imposed in the long direction of the container (l = 950 mm), and the cyclic loading amplitude was alternated between ±3mm of displacement at pile head. Furthermore, **Fig. 6** shows that the frequency of the lateral cyclic displacement was in range of 0.017 Hz and 0.05 Hz which simulates the impact of loading of wind and waves on the offshore structures supported on mono-pile foundations in most of the coastal regions (refer to Natarajan et al., 2015).

For the purpose of facilitating the visualization of the soil movements during testing and image processing, SONY Cyber-shot Camera with resolution 20.1

megapixel was used, as shown in **Fig. 7**. Based on photo image analysis technique, photo shoots have been taken for the deformations of soil particles and colored grid lines during 50 cycles of loading (N = 50).

3.2 Mesh grid on the top of soil surface

After placement of the top layer of the Toyoura sand inside the testing container, it was colored with red grid lines which are placed in short (h = 300 mm) and long (l = 950 mm) directions the top side of the testing chamber (i.e., parallel and perpendicular to cyclic load direction, as shown in **Figs. 8** and **9**, respectively). Thin grid lines have been installed using colored soil at equal and parallel offsets distance equal B (pile diameter), then the spacing was increased to 2B in the middle of the testing chamber, and near the outer boundaries of the chamber the grid lines were placed at spacing of 3B.

4. Analyses of results

Estimation of the 3D conical failure zone around pile shaft due to lateral loading was carried out via two steps, including: (1) determination of the range of lateral plastic deformations at the top of ground surface in both of perpendicular and parallel directions of cyclic loads; and (2) determination of the point of rotation (zero displacement) along the pile shaft. The former step was performed using photo image analysis technique, while the later step was performed using an analytical method based on cyclic p-y curve technique.

4.1 Lateral plastic deformation

Figure 10 illustrates the shape of the deformed grid lines (perpendicular to loading direction) around pile shaft after 50 cycles. It was found that the grid lines perpendicular to cyclic loading direction experienced plastic deformations to extent of twice the diameter of the pile (2B) measured from the centerline of pile diameter. On the other hand, **Fig. 11** depicts the deformed grid lines on the top surface of soil in direction parallel to the cyclic loading direction. It is obvious that the lateral plastic deformations occurred to a distance of three times pile diameter (3B) measured from the centerline of pile diameter.

4.2 Cyclic p-y curve

Pile lateral displacement (y) and soil reaction (p) were determined by double integration and double derivation of moment curves along the pile shaft, as given by Eqs. 10 and 11, respectively. The boundary conditions adopted to solve the equations were the measured displacement at pile head and zero bending moment at pile tip (Awad-Allah and Yasufuku, 2013).

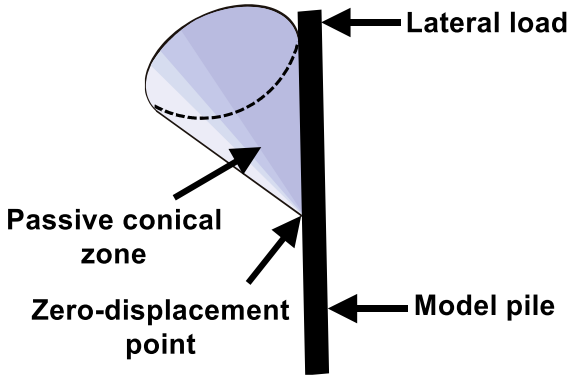

Fig. 3. Definition of failure zone (after Otani et al., 2006).

Table 1. Geotechnical properties of Toyoura sand.

Property	Value
Specific gravity (G_s)	2.65
Maximum dry unit weight (γ_{max})	16.0 kN/m^3
Minimum dry unit weight (γ_{min})	13.1 kN/m^3
Maximum void ratio (e_{max})	0.98
Minimum void ratio (e_{min})	0.62
Uniformity coefficient (U)	1.40
Coefficient of curvature (C)	0.86
Effective diameter (D_{50})	0.18 mm

Table 2. Equivalent values for the characteristics of prototype and experimental model.

Parameter	Prototype	Model
Material	Steel	Aluminum
Modulus of elasticity of pile material (E_P)	200 GPa	70 GPa
Diameter of pile (B)	600 mm	15 mm
Load eccentricity (e)	4.07 m	0.1 m
Pile embedded length (L)	12.2 and 18.3 m	0.30 and 0.45 m
Modulus of elasticity of soil (E_s)	18.6 MPa	6.48 MPa

$$y(z) = \frac{1}{EI}\iint M(z)dz^2 \quad [10]$$

$$p(z) = \frac{d^2M(z)}{dz^2} \quad [11]$$

where: M(z) = measured bending moment along the pile length.

It was found in the literature that the initial stiffness of the p-y curves is highly depending on the pile diameter

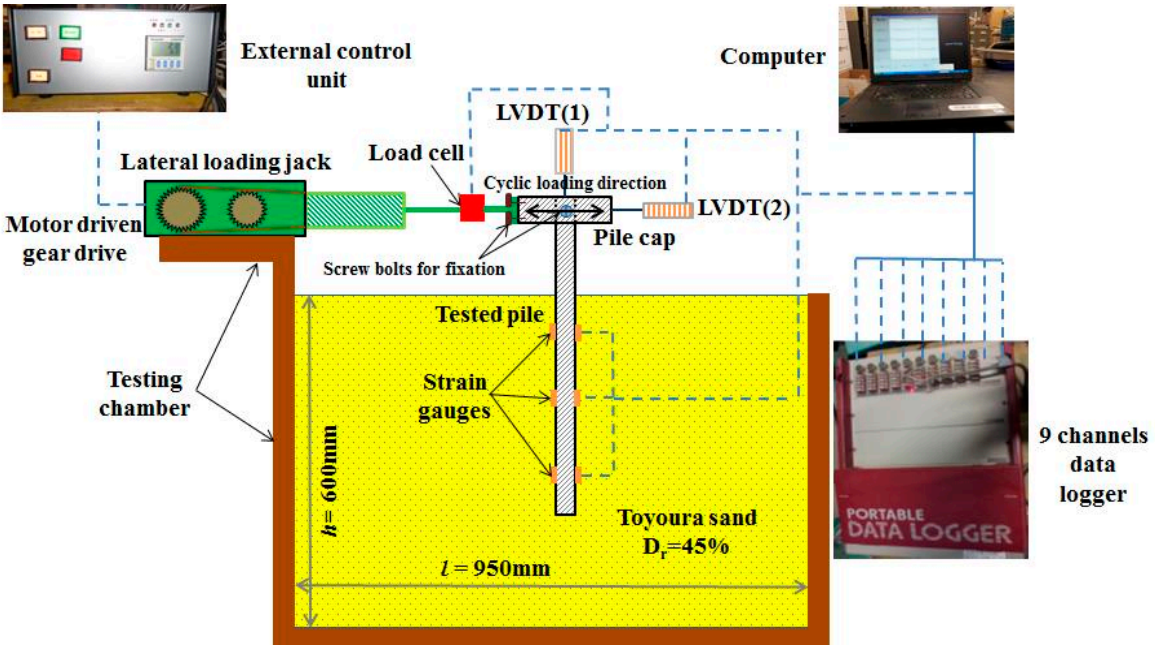

Fig. 4. Schematic of experimental setup.

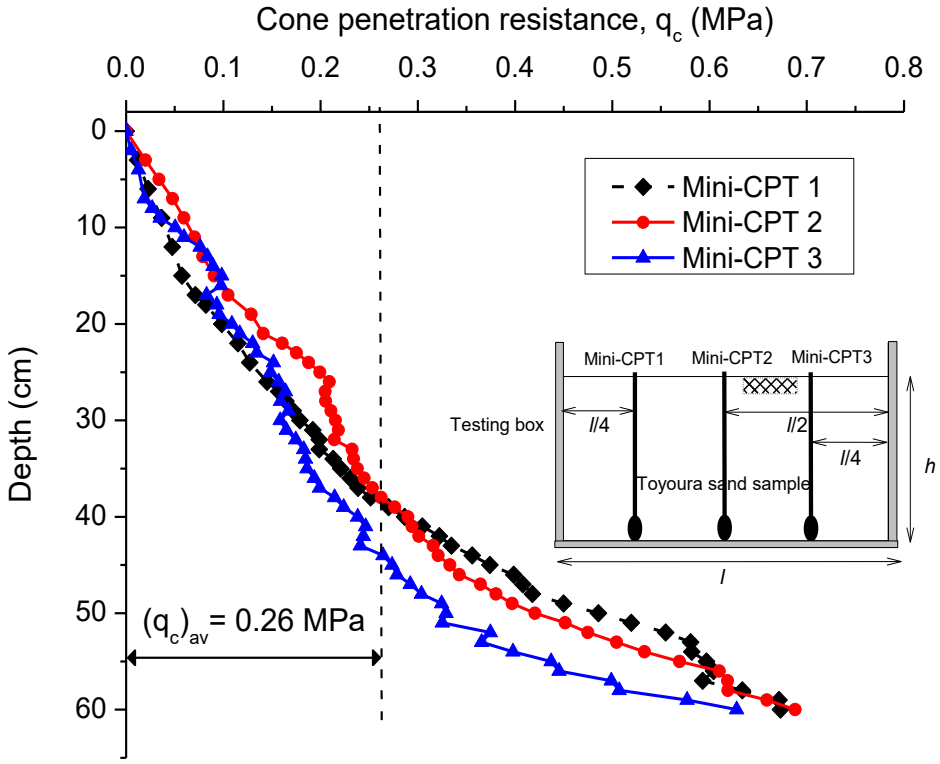

Fig. 5. Results of the three Mini-CPT tests over the depth of the soil testing box.

and soil stiffness (see, e.g. Kagawa and Kraft, 1981; Bhattacharya et al., 2011; Klar, 2008; etc.).

Consequently, in this study the lateral reaction (p) and lateral displacement of soil (y) were normalized with respect to soil unit weight of soil (γ) and pile diameter (B), as follows:

$$p^{-} = \frac{p}{\gamma * B^2} \quad [12]$$

$$y^{-} = \frac{y}{B} \quad [13]$$

Because the performance of flexible piles (L/B = 20 and 30) revealed almost similar trend during cyclic

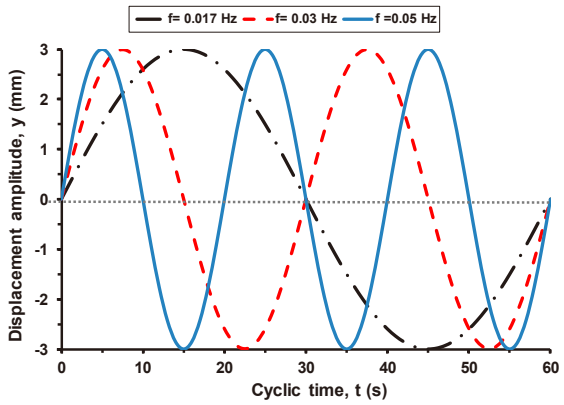

Fig. 6. Two-way lateral cyclic displacement of three different frequencies.

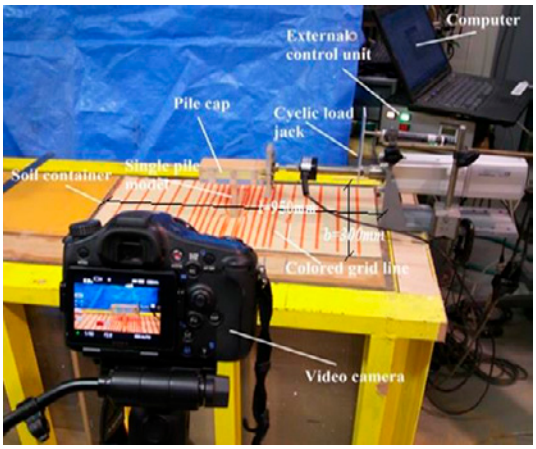

Fig. 7. Monitoring of soil deformation at top soil using video image analysis.

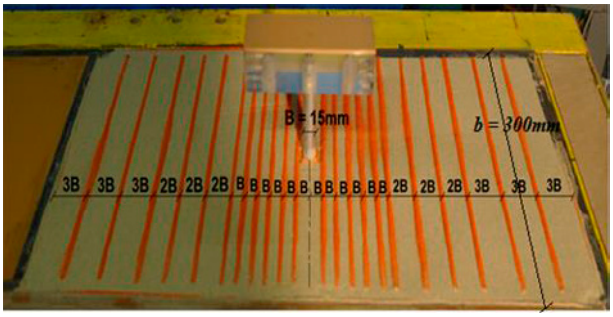

Fig. 8. Grid lines on top soil in short direction (b = 300mm) of the testing box.

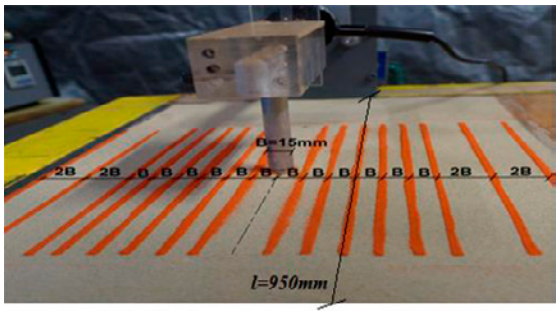

Fig. 9. Grid lines on top soil in long direction (l = 950mm) of the testing box.

loading, only the cyclic p-y curves for flexible piles of L/B = 20 were introduced herein. **Figures 12** and **13** illustrate the cyclic p-y curves for pile of L/B = 20 at two different soil layers at depths of 6B and 15B measured from ground surface, respectively. **Figure 12** depicts that, for soil layer at level of z ≤ 6B, magnification of p-y curves has been observed due to increase of the number of cycles N up to 50 cycles. On the other hand, **Fig. 13** shows that, at deeper soil layer at level z ≥ 15B from ground surface, degradation of p-y curves has been observed due to increase of number of cycles N up to 50 cycles. It is also noticed that effect of loading frequency (f) has a relatively little impact on degradation and magnification of cyclic p-y curves.

4.3 Determination of point of rotation of along pile shaft

Since the pile models employed in this study were flexible piles, their points of rotations (plastic hinge points) were created at locations beneath the ground surface where the lateral soil displacements were equal to zero. This indicates that at those locations no change in the soil reactions (p) will occur due to lateral cyclic loading (i. e., $p_1 \approx p_N$). Moreover, it is noticeable that p-y curves are affected and changed by the elevation of the soil layer from the ground surface at which p-y curve is estimated (see, e.g. Rosquoet et al; 2007, Padmavathi, et al.; 2008, and Awad-Allah et al.; 2014). Thus, lateral soil reaction due to lateral cyclic loading can be represented as function of degradation or magnification factors (r) with respect to the depth of soil stratum. These factors were calculated using Eq. 14.

$$r = \frac{p_1}{P_N} \qquad [14]$$

where: r = degradation and magnification factors, p_1 = the peak soil reaction mobilized during monotonic test after 1st cycle, and p_N = the corresponding soil reaction mobilized during cyclic test after Nth cycles.

Consequently, one of the following three cases can be arisen from Eq. 14: r = 1 ($p_1 = p_N$, point of rotation is created at this location; r < 1 ($p_1 < p_N$, degradation of p-y curve has occurred at that location); and r > 1 ($p_1 > p_N$) magnification of p-y curve has occurred at that location).

Figure 14 shows the variation of r-factor with the elevation of soil layer with respect of ground surface, frequency of loading, and number of cycles. It is obvious that (r) values were markedly affected by the layer depth and the number of cycles. For the layers at depths between 3B and 6B from ground level, r-factors

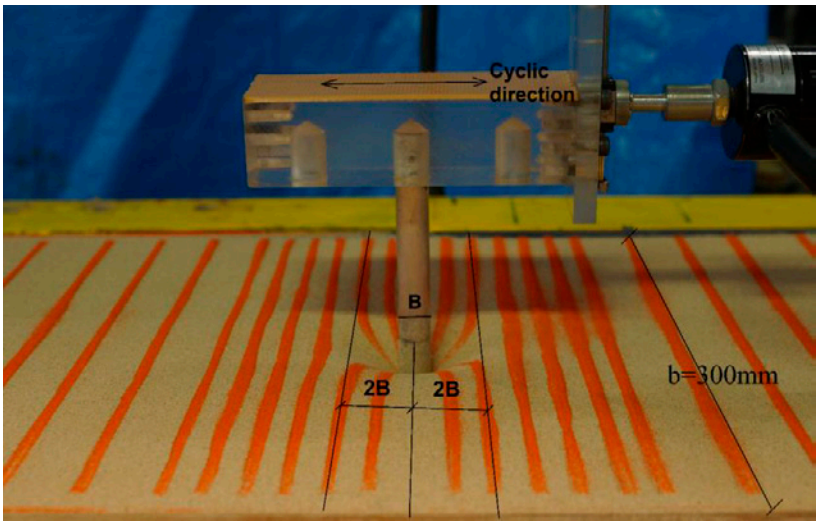

Fig. 10. Deformed grid lines on top soil in short direction of the testing box b = 300 mm (perpendicular to cyclic load) after 50 loading cycles.

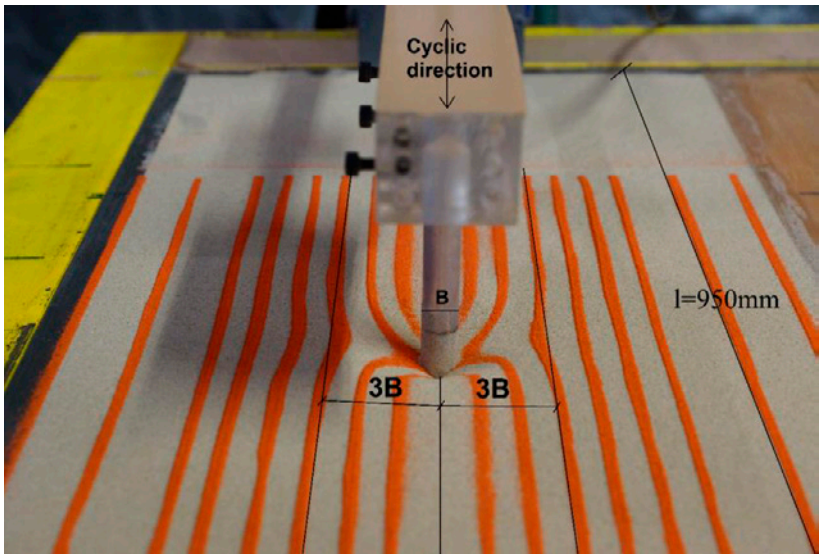

Fig. 11. Deformed grid lines on the top surface of soil l = 950 mm (direction parallel to the cyclic loading). The lateral plastic deformations occurred to a distance of three times pile diameter (3B) measured from the centerline of pile diameter

increased with increasing number of cycles (all values are greater than 1). On contrast, for the layers at depths between 10B and 15B from ground level, reduction of r-factors occurred with increasing the number of cycles. As a result, for pile subjected to lateral cyclic loading, the point of zero displacement (point of pile rotation) is created at pile length of 9B measured form the ground surface where the r-factor is almost equal to the unity (1).

5. Proposed 3D conical failure zones due to cyclic load

Based on the previous analysis, 3D failure zone is characterized by the mobilized base angles (β_m and α_m) which define the wedges of soil failure in two perpendicular directions. The base angle β_m was mobilized in the parallel direction to the cyclic loading excitation, and it gave value of 9.5° which is about 0.26φ (where: φ is the internal friction angel of medium dense sand soil which is equal to 36.5°). However, the second base angle α_m was mobilized in the perpendicular direction to the cyclic loading excitation, and it gave value of 15.5° which is about 0.42φ, as shown in **Fig. 15**.

It is clear that the 3D deformed shape gave a form of cone which has an ellipse on the top and a height of 9B (point of pile rotation) where the cyclic "p-y" curves response changed. The height of conical shape is measured form the top soil surface to the point of pile rotation (i.e. point of zero lateral displacement). Furthermore, the shape of the ellipse on the top soil surface has major and minor axes of 6B and 4B,

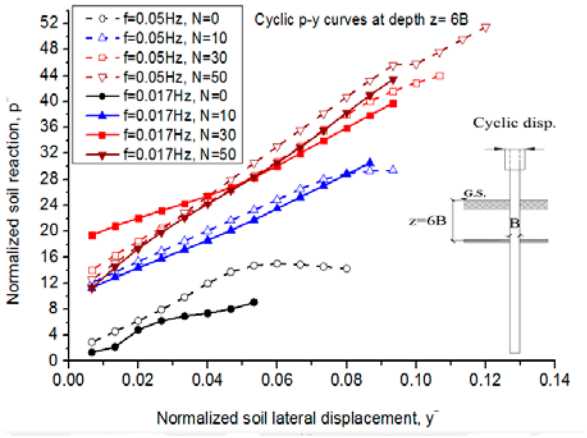

Fig. 12. Normalized cyclic p-y curves at (z/B = 6) for piles in medium dense sand (D_r = 45%).

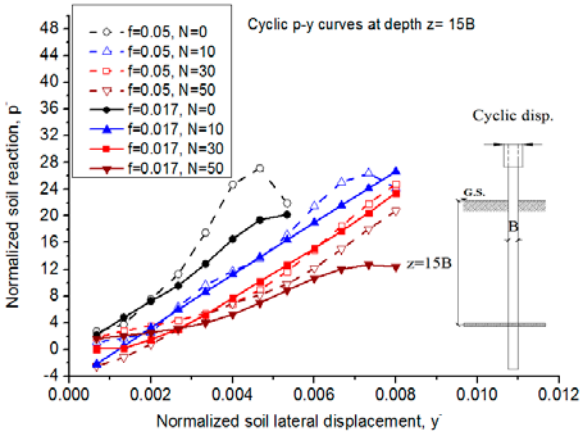

Fig. 13. Normalized cyclic p-y curves at (z/B =15) for piles in medium dense sand (D_r = 45%).

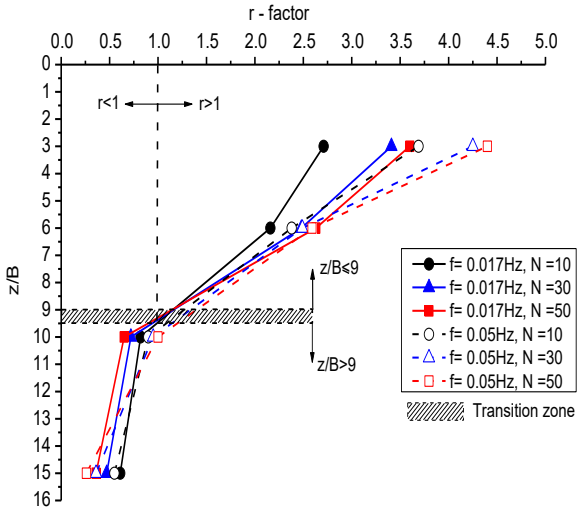

Fig. 14. Change of magnification and degradation factors (r) with soil layer depth, loading frequency f, and number of cycles N.

respectively, measured from the center line of the pile diameter. The whole deformations occurred in the radial direction (i.e., in the direction of pile diameter). As a result, **Fig. 16** illustrations the proposed 3D conical failure zones around the pile shaft due to lateral cyclic loading based on photo image analysis and cyclic p-y curve techniques.

It is worth to mention the limitation and validity of application of the proposed 3D conical failure model in engineering practice. The following two conditions that should be fulfilled so that the proposed model being valid in the practice: (1) pile/soil relative stiffness (E_p/E_s) has to be equal to $10*10^{-3}$, and (2) loading frequency (f) has to be in range of 0.017 to 0.05 Hz.

6. Summary and conclusions

In the paper, small-scale single pile models installed into medium dense sand soil conditions and subjected to two-way lateral cyclic loading of excitation range of 0.017 to 0.05 Hz has been introduced. The main aim of the paper is to determine the 3D conical failure zone around pile shaft due to lateral loading via two steps, including: (1) determination of the extent of lateral plastic deformations at the top of ground surface in perpendicular and parallel directions of cyclic loads; and (2) determination of the point of rotation (zero displacement) along the pile shaft. Furthermore, 3D failure patterns adjacent to pile shaft were determined using photo image analysis and analytical methods. The following conclusions are drawn:

I. The lateral plastic deformations around single pile shaft subjected to lateral cyclic loading were experimentally investigated using photo image analysis. The plastic deformations created on the top soil surface were extended laterally as a shape of ellipse with major and minor axes of 6B and 4B after applying 50 two-way lateral cyclic loading.

II. The proposed 3D conical failure zone was characterized by two base angles (β_m and α_m), which define the wedges of soil failure in two perpendicular directions, as well as by the depth of the point of pile rotation.

III. In engineering practice, for grouped piles installed in medium dense sand and subjected to lateral cyclic loading of frequency range of 0.017 to 0.05 Hz, the spacing between centers of piles in the group should be kept at distance of 3B to avoid the interaction between the failure zones.

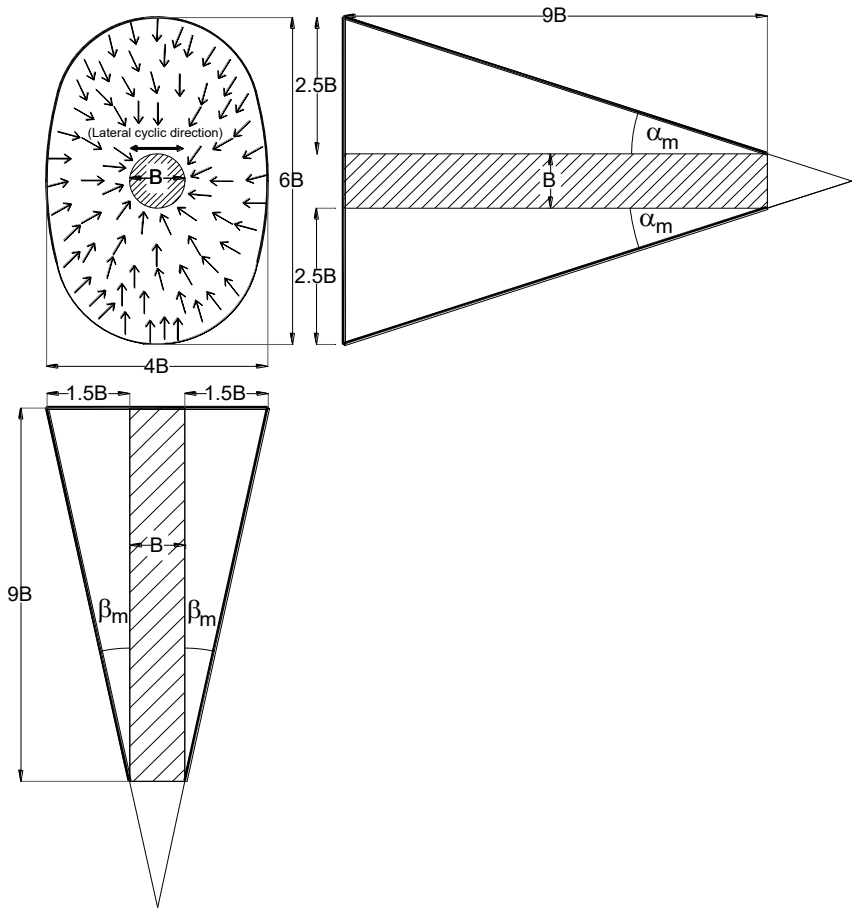

Fig. 15. Plastic deformations boundaries at soil top surface around lateral cyclic loaded pile and the mobilized base angles for the wedges of soil failure.

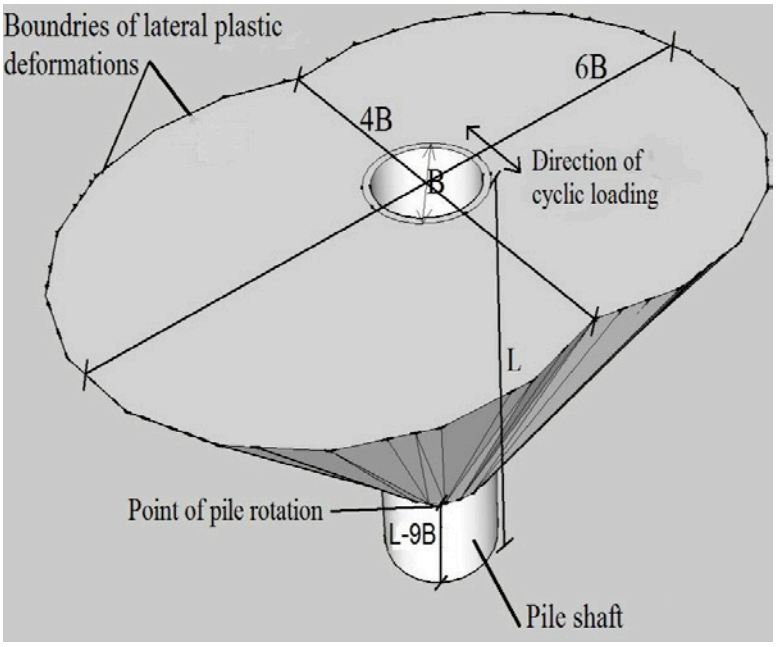

Fig. 16. Three dimensional (3D) conical failure zone around pile shaft due to lateral cyclic loading in medium dense sand (D_r = 45%).

References

Abedzadeh, F. and Pak, R.Y.S., 2004. Continuum mechanics of lateral soil-pile interaction. Journal of Engineering Mechanics, ASCE **130** (11): 1309-1318.

Ashour, M., Norris, G. and Pilling, P., 1998. Lateral loading of a pile in layered soil using the strain wedge model. J. Geotech. Geoenv. Engrg., **124** (4): 303-315.

Awad-Allah, M.F. and Yasufuku, N., 2013. Performance of pile foundations in sandy soil under slow cyclic loading. The 5th Intl. Conf. Geotechnical Symposium on Geot. Eng. for Disaster Prevention & Reduction, May 2013, Korea: 291-300.

Awad-Allah, M.F., Yasufuku, N. and Abdel-Rahman, A.H., 2014. Factors controlling the behavior of piled foundations due to cyclic lateral loading. Proc. the 6th Japan-Taiwan Joint Workshop on Geotechnical Hazards from Large Earthquakes and Heavy Rainfalls, July 2014, Kitakyushu, Japan: 555-568.

Basack, S. and Purkayasthab, D., 2007. Behavior of single pile under lateral cyclic load in marine clay. Asian Journal of Civil Engineering, **8** (4): 443-458.

Bhattacharya, S., Lombardi, D. and Wood D., 2011. Similitude relationships for physical modelling of monopile-supported offshore wind turbines. Intl. J. Physical Modelling in Geotechnics, **11** (2): 58-68.

Chandrasekaran, S., Boominathan, A. and Dodagoudar, R., 2010. Experimental investigations on the behavior of pile groups in clay under lateral cyclic loading. Geotechnical and Geological Engineering, **28** (5): 603-617.

Fleming, W.G.K., Weltman, A.J., Randolph, M.F. and Elson, W.K., 2009. Piling Engineering, Taylor and Francis, London and New York.

Japanese Geotechnical Society, 2003. JGS 1431. Portable cone penetration test. Tokyo, Japan.

Kagawa, T. and Kraft, L.M., 1981. Dynamic characteristics of lateral load-deflection relationships of flexible piles. Earthquake Engineering & Structural Dynamics, **9** (1): 53-68.

Kishida, H. and Nakai, S., 1979. Analysis of a laterally loaded pipe with non-linear subgrade reaction. Transaction of Architectural Institute of Japan, **281**: 41-55 (in Japanese).

Klar, A., 2008. Upper bound for cylinder movement using 'elastic' fields and its possible application to pile deformation analysis. International Journal of Geomechanics, ASCE, **8** (2): 162-167.

Lombardi, D., Bhattacharya, S., Fabrizio, S. and Bianchi, M, 2015. Dynamic response of a geotechnical rigid model container with absorbing boundaries. Soil Dynamics and Earthquake Engineering, **69**: 46-56.

Masoud, H., Yones, S. and Habin, A., 2011. Soil deformation pattern around laterally loaded piles. International J. of Physical Modelling in Geotechnics, 11 **(3)**: 116-125.

Miura, S. and Toki, S., 1982. A simple preparation method and its effect on static and dynamic deformation-strength properties of sand. Soils and Foundations, **22** (1): 61-77.

Natarajan, M., Mohan, K. and Balasubramanian, T., 2015. Waves and tides, Centre of Advanced Study in Marine Biology, Annamalai University, Tamil Nadu, India. Diana Morales: 32-44. http://www.scribd.com/doc/252783539/WavesandTidesscribd.

Nikudel, M.R., Mousavi, S.E., Khamehchiyan, M. and Jamshidi, A., 2012. Using miniature cone penetration test (Mini-CPT) to determine engineering properties of sandy soils. J. Geopersia, **2** (2): 65-76.

Ovesen, N.K., 1975. Centrifugal testing applied to bearing capacity problems of footings on sand. Geotechnique **25** (2): 394-401.

Otani, J., Pham, K.D. and Sano, J., 2009. Investigation of failure patterns in sand due to laterally loaded pile using x-ray CT. Soils and Foundations, **46** (4): 529-535.

Padmavathi, V., Saibaba Reddy, S. and Madhav, M.R., 2008. Behaviour of laterally loaded rigid piles in cohesive soils based on kinematic approach. Lowland Technology International Journal **10** (1): 27-41.

Poulos, H.G. and Davis, E.H., 1980. Pile foundation analysis and design. John Wiley & Sons, New York, NY, USA.

Reese, L.C., Cox, W.R. and Koop, F.D., 1974. Analysis of laterally loaded piles in sand. Proc. 6th Annual Offshore Technology Conference, Houston, **2**: 473-484.

Reese, L.C., 1977. Laterally loaded piles. Program Documentation. J. Geotech. Engrg. Div., American Society of Civil Engineers (ASCE), **103** (GT4) Proc. Paper 12862: 287-305.

Wood, D.M., 2004. Geotechnical Modelling. Applied Geotechnics. Spon Press, London, UK, **1**.

LeBlanc, C., Byrne B.W. and Houlsby G.T. 2010. Response of stiff piles in sand to long term cyclic loading. Geotechnique, **60** (2): 79-90.

Rosquoet, F., Thorel, L., Garnier, J. 2007. Lateral cyclic loading of sand-installed piles. Soils and Foundations, **47** (5): 821-832.

Symbols and abbreviations

B	Pile diameter
C	Coefficient of curvature
D_{50}	Effective diameter
D_W	Passive wedge depth
EI	Bending (flexural) stiffness of pile
E_m	Modulus of elasticity of model pile
E_P	Modulus of elasticity of prototype pile
E_s	modulus of elasticity of soil
E_P/E_s	Pile/soil relative stiffness
e_{max}	Maximum void ratio
e_{min}	Minimum void ratio
$F= L_p/L_m$	Scale factor for length
f	Loading frequency
G_s	Specific gravity
h	Width of testing box
I_m	Moment of inertia of model pile
I_p	Moment of inertia of prototype pile
K_h	Modulus of subgrade reaction of soil
$(K_h)_s$	Secant modulus of subgrade reaction of soil
K_p	Passive earth pressure coefficient
K_{rs}	Relative stiffness factor
L	Embedment length of pile
l	Length of testing box
M(z)	Measured bending moment along the pile length
N	Number of cycles
n_h	Coefficient of subgrade reaction
p_u	Ultimate soil lateral resistance
p_1	Soil reactions for 1st cycle of loading
p_N	Soil reactions for Nth cycle of loading
p^-	Normalized soil reaction
r	Degradation and magnification factor
t	Time
U	Uniformity coefficient
y	Lateral displacement of pile
y^-	Normalized lateral soil displacement
z	Depth below ground soil level
α_m	Mobilized base angles in the parallel directions to cyclic loading
β_m	Mobilized base angles in perpendicular direction of cyclic loading
φ	Internal friction angle
φ_m	Mobilized friction angle
ϕ_1	Natural dimensionless ratio
γ	Unit weight of soil
γ_{max}	Maximum dry unit weight
γ_{min}	Minimum dry unit weight
σ_y	Yield stress of pile material
$\Delta\sigma_h$	Horizontal stress change at the passive wedge
τ	Side shear (τ) act on the strain wedge